Acta Cryst. (1997). A53, 632–642

High-Order Supersatellite Reflections in Labradorite. A Synchrotron X-ray Diffraction Study

MARKUS KALNING,[a] VOLKER DORNA,[a] BERND BURANDT,[a] WERNER PRESS,[a] STEFAN KEK[b]* AND HANS BOYSEN[c]

[a]*Institut für Experimentalphysik, Universität Kiel, D-24098 Kiel, Germany,* [b]*FR Kristallographie, Universität des Saarlandes, D-66041 Saarbrücken, Germany, and* [c]*Institut für Kristallographie und Mineralogie, Universität München, München, Germany. E-mail: kek@vxdesy.desy.de*

(*Received 5 December 1996; accepted 11 June 1997*)

Abstract

The supersatellite reflections in the feldspar mineral labradorite are related to the Bøggild intergrowth, a lamellar structure with a periodicity of about 1500 Å. With high-resolution X-ray diffraction using synchrotron radiation, supersatellites up to fourth order are observed. The system is an example for a natural superstructure with high-order diffraction harmonics. The satellite intensities reflect a transverse displacement modulation with a large amplitude. The complete unit cell of labradorite is affected by the displacement. In this context, various possible displacement functions are discussed. A Fourier expansion of the displacement function that yields the best agreement between measurement and theory has nearly triangular shape. The line width of the satellites characterizes imperfections of the lamellar superstructure: It increases linearly with satellite order, which is ascribed to uncorrelated variations (FWHM = 480 Å) of the lamellar thickness.

1. Introduction

Labradorite crystals often show a colourful iridescence arising from a lamellar structure, the Bøggild intergrowth (Bøggild, 1924), with periodicities of around 1500 Å. The satellite reflections related to this superstructure are the subject of the present study. They were first observed by Jagodzinski & Korekawa (1965) and called s-satellites (supersatellites) by them. Burandt, Komorek, Press & Boysen (1992) gave a first quantitative analysis of the satellite intensities: They were analysed within a model of a harmonic transverse displacement modulation of the entire unit cell, accompanied by a harmonic density modulation. A displacement amplitude of 0.75 Å was obtained. Therefore, this modulation has been called a 'frozen-in' transverse acoustic (TA) phonon. The contribution of the density modulation to the intensities turned out to be less than 2% of the unmodulated structure factor and hence is insignificant. This investigation was based on a relatively small data set of 25 a-reflections (see below for definition) and their satellites collected at a laboratory X-ray diffractometer and the data were restricted to only two different scattering planes. The limited amount of data was due to the fact that enhanced resolution is required to separate the supersatellites from the main peaks. In continuation of this study, a larger high-resolution data set was measured with synchrotron radiation at the four-circle diffractometer at the HASYLAB beamline D3. With special care taken of the experimental parameters at the four-circle diffractometer, satellites up to fourth order were observed. The data set includes reflections at rather high momentum transfers. It is well suited for an investigation of both the intensities and the line shapes of the supersatellite reflections. From the intensities of the higher-order supersatellite reflections, more information on the modulation can be expected: It may be possible to identify displacements of individual atoms, indicating other mode eigenvectors with the same symmetry as the frozen-in TA phonon. So far, the displacement function was assumed to be purely harmonic. The large amplitude of the displacement function suggests, however, that anharmonic terms may also be significant. It was one of the goals of the present investigation to learn about the importance of higher-order contributions to the displacement function. Additionally, the line shape of the supersatellite reflections contains information about the degree of perfection of the lamellar superstructure.

Some introductory remarks concerning previous studies on the structure of labradorite appear necessary: In the intermediate plagioclases, only main reflections with indices $h + k = 2n$ and $l = 2n$, called a-reflections, occur. In labradorite, supersatellites accompany all a-reflections. So-called b-reflections ($h + k = 2n + 1$ and $l = 2n + 1$) are absent, but symmetrical to their positions e-satellites are found, while second-order satellites (often called f-satellites) surround the a-reflections. This e-type modulation has been observed and discussed controversially in the literature for more than four decades. Its period is about 30–60 Å and this superstructure is mainly connected with a tendency towards Al–Si order (Toman & Frueh, 1976). Various models are based on antiphase domains (Horst, Tagai, Korekawa & Jagodzinski, 1981) or the formation of albite- and anorthite-rich regions (Yamamoto, Nakazawa, Kitamura & Morimoto, 1984). We have recently reinvestigated the e-type modulation using synchrotron data. This will be published in a

separate paper (Kek, Kalning, Press, Boysen & Frey, 1997).

As pointed out by Jagodzinski (1984), these results represent a coherent superposition of the structures of two types of Bøggild lamellae, since they do not consider the s-satellites. Apart from the (only) X-ray observation of the s-modulation of Jagodzinski & Korekawa (1965), there are various transmission electron microscope (TEM) investigations (*e.g.* Wenk & Nakajima, 1988; Smith & Brown, 1980; Hoshi, Tagai & Suzuki, 1996). They reveal a lamellar structure with varying thicknesses and rough interfaces. Ion-probe measurements (Miúra & Tomisaka, 1978), as well as the recent TEM study of Hoshi, Tagai & Suzuki (1996), show that the An content in the two lamellae differs by about 10%. It should be mentioned that labradorites exhibiting the schiller effect always contain about 2–4% of orthoclase, which also seems to differ slightly in the two lamellae. The motivation to perform a quantitative X-ray analysis of the s-modulation is that finer structural details may be derived and thermodynamically more relevant averages are determined (instead of the more local information of the TEM investigations). A fully conclusive description of the superstructures in labradorite should include both modulation types simultaneously. Two different situations are conceivable: (i) The e-modulation is continuous over the whole crystal. In this case, supersatellites should accompany the e-reflections. (ii) The e-modulation is characteristic for each s-lamella. In this case, two (broadened) e-satellites with slightly different orientation and position should be observed. Two-dimensional Q scans over the e-satellites (Kek *et al.*, 1995) clearly reveal that case (ii) applies, in agreement with TEM. Collecting a complete data set of both types of satellite simultaneously would be an enormous task, even at a synchrotron, apart from the difficulty of separating the superimposed two e-reflections. Nevertheless, the basic principles of the superstructure may be determined by treating both types separately, if one keeps in mind that for the s-type this means an *average* over the e-modulation is taken (non-consideration of e-satellites), while for the e-type an *ideal* structure (as if no s-modulation exists: here integrated a-intensities, including the s-satellite intensities, are used) is considered.

The present paper is organized as follows: §2 deals with the calculation of the intensity distribution of the satellites. We derive analytical solutions for rectangular and triangular displacement functions and compare these with the result of a Fourier expansion of the displacement function. §3 describes experimental details and the quality of the measured data. A discussion of the ψ rotation, which plays a crucial role in obtaining well resolved data, is given in Appendix *A*. In §4, the measured intensities are analysed and, in §5, the results are discussed. In addition, we give an interpretation of the measured line width.

2. Theory

A modern description of modulated structures in higher-dimensional space has been introduced by de Wolff (1974, 1977), Janner & Janssen (1977) and de Wolff, Janssen & Janner (1981). Recently, considerable work has been done in analysing incommensurately modulated structures within the superspace formalism (Yamamoto, 1982*a*,*b*; Petříček *et al.*, 1991; Lam, Beurskens & van Smaalen, 1994), the last including higher harmonics. The importance of higher harmonics in the analysis of modulated structures has been emphasized by Jagodzinski (1984), with special regard to the feldspar minerals. Various program packages are now available for the refinement of modulated structures. Test refinements have been done using *JANA*94 (Petříček, 1994). The superspace group is $P\bar{1}^{P1}$ with non-standard centring vectors $(\frac{1}{2}\frac{1}{2}\frac{1}{2}0)$, $(\frac{1}{2}\frac{1}{2}00)$ and $(00\frac{1}{2}0)$, to keep the common practise of describing intermediate plagioclases within the anorthite cell (*i.e.* $c \simeq 14$ Å). Allowing for various degrees of freedom, individual modulation waves for different (groups of) atoms, sine and cosine terms, and occupational wave for Ca/Na, the refinements finally showed that a purely transverse displacive modulation of the *entire* unit cell (*i.e.* no individual phases) is sufficient to fit the observed intensities satisfactorily [thus justifying the assumptions of Burandt *et al.* (1992)]. Owing to the limited data set (see below), all other degrees of freedom were hardly significant. To reduce the number of free parameters, various restrictions can be imposed in *JANA*.

The data set suitable for the *JANA* refinement was available after scaling with integrated a-reflection intensities, measured by Kek *et al.* (1997). Before this combined data set was available, a rather simple model was used, which can easily be described using and extending the 'classical' satellite theory of Korekawa (1967*a*,*b*), which is equivalent to the superspace formalism and is more directly applicable to discuss various *shapes* and their influence on the intensities. Moreover, this approach yields quantitative results on the basis of *relative* intensities of satellites *versus* main reflections. These relative intensities of the various satellite orders are available directly from the experiment (see below).

Since the density modulation turned out to be of little significance (see above), we restrict ourselves to a description in terms of displacement modulations of a sinusoidal, a rectangular and a triangular displacement function. Finally, an extension is made to the more general case of a Fourier series for the displacement function.

Intensity formulae for the three types of shape function have been derived by Böhm (1976, 1977) and are briefly repeated here. In the following, $\mathbf{Q}_{\rm mod}$ denotes the satellite vector and $\mathbf{B}$ the displacement vector, which is perpendicular to $\mathbf{Q}_{\rm mod}$ in the case of a purely transverse

modulation. $\mathbf{Q}_\perp$ denotes the component of a reciprocal-lattice vector in the direction of **B**.

For the *transverse harmonic displacement modulation*, the intensities are proportional to squares of Bessel functions of order n, with n denoting the satellite order and $n = 0$ the main reflection:

$$I_n = |F_0|^2 J_n^2(\mathbf{Q}\cdot\mathbf{B}) = |F_0|^2 J_n^2(\mathrm{Q}_\perp B). \qquad (1)$$

$F_0 = F_0(\mathbf{Q})$ is the structure factor of the (unmodulated) unit cell. The vector description also holds for a longitudinal displacement or any other direction of **B**. The harmonic displacement modulation is always useful as a first approximation of an arbitrary displacement function, which appears smooth, for example due to the averaging over a larger sample area.

A *rectangular displacement modulation* corresponds to crystalline domains, transversely shifted against each other by an amplitude B (see Fig. 1). The resulting scattering amplitude is

$$|S_{\mathrm{MR}}| = |F_0|[1 + 4(D_1/M)(D_1/M - 1)\sin^2(\mathrm{Q}_\perp B)] \quad (2)$$

for the main reflection and

$$|S_{\mathrm{sat},n}| = |F_0|\left|\frac{2\sin(\mathrm{Q}_\perp B)\sin(\pi n D_1/M)}{M\sin(\pi n/M)}\right|$$

for the satellites $n = \pm 1, \pm 2, \ldots$. $M = D_1 + D_2$ is the period of the modulation in direct space. D_1 and D_2 denote the widths of adjacent lamellae. For a symmetrical modulation ($D_1/M = 0.5$), the satellites of even order are absent. Generally, the first-order satellite is stronger than the higher-order satellites in the rectangular case.

The triangular modulation is parametrized (asymmetric with two different slopes) as shown in Fig. 1:

$$g(x) = \begin{cases} a_1(x - 1/2) & 0 \le x \le (D_1' + 1)/2 \\ a_2(M'/2 + 1/2 - x) & \\ & (D_1' + 1)/2 \le x \le M' - (D_1' + 1)/2 \,. \end{cases} \qquad (3)$$

D_1' and D_2' denote the widths of the two adjacent domains, a_1 and a_2 are the slopes of the displacement function. The following relations hold: $a_1 = 2B/D_1'$; $a_2 = 2B/D_2'$; with $D_1' + D_2' = M'$.

The scattering amplitude then reads:

$$|S_{\mathrm{sat},n}| = |F_0||\{\sin[(a_1 + a_2)\mathrm{Q}_\perp/2] \times \sin(\pi D_1' n/M' + \mathrm{Q}_\perp B)\} \times [M'\sin(\pi n/M' + \mathrm{Q}_\perp B/D_1') \times \sin(\pi n/M' - \mathrm{Q}_\perp B/D_2')]^{-1}|, \quad n = 0, \pm 1, \pm 2, \ldots. \qquad (4)$$

Note that a difference in the width of the neighbouring lamellae ($D_1 \neq D_2$) yields different intensities for pairs of satellites of order $\pm n$. Conversely, for identical widths, a symmetric intensity distribution is observed. A triangular modulation can be associated with twinned domains, for example.

The intensities for main reflections and satelites up to fourth order, resulting from these three cases, as described by equations (1), (2) and (4), are compared in Fig. 2. For simplicity, a Q-independent structure factor F_0 and the same widths for the adjacent lamellae ($D_1 = D_2$, $D_1' = D_2'$) have been assumed. Note that the intensities are plotted *versus* $|\mathbf{Q}\cdot\mathbf{B}|$ and not simply *versus* $|\mathbf{Q}|$. The rectangular displacement yields main reflections whose intensity is periodic in $|\mathbf{Q}\cdot\mathbf{B}|$ with maximum intensity at $|\mathbf{Q}\cdot\mathbf{B}| = 2\pi l$ (l integer). In between these positions, satellites occur, with the first-order satellites dominating in the symmetric case. For the sinusoidal displacement, the intensity of the main reflection is proportional to J_0^2 and hence damped compared with that of the unmodulated structure. For the triangular modulation, the main reflections are more strongly damped and the intensities of higher-order satellites increase with increasing $|\mathbf{Q}\cdot\mathbf{B}|$. Simulated curves for Q scans along the direction of modulation are given in the respective inserts in Fig. 2. They are calculated assuming a resolution-limited width for the main reflection and a constant broadening for the satellites. Note the close similarity between the harmonic and the triangular displacement.

A more general approach, which includes the analytical solutions given above as special cases, is obtained by use of a Fourier expansion of the shape function. This approach is useful, since the high-order Fourier components of the shape function are not accessible in the measurement. A similar access is used in some higher-dimensional approaches such as *JANA* (Petříček, 1994). Within the kinematical description, the scattering amplitude $S(\mathbf{Q})$ is given by

$$S(\mathbf{Q}) = F(\mathbf{Q})\sum_n \exp(-i\mathbf{Q}\mathbf{r}_n).$$

$F(\mathbf{Q})$ denotes the structure factor of the undisplaced unit cell, $\sum_n$ is the summation over all unit cells of the

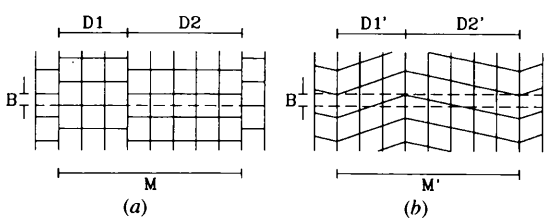

Fig. 1. Illustration of the parameters describing (*a*) the rectangular displacement and (*b*) the triangular displacement. While the rectangular displacement describes transversely shifted domains, the triangular displacement can be due to twinning or a mismatch of lattice parameters.

crystal and $\mathbf{r}_n$ is the origin of the nth unit cell (as we restrict ourselves to a modulation of the entire unit cell).

In the case of a one-dimensional modulation, the unit cells are displaced periodically as a function of $\mathbf{Q}_{\text{mod}}$ relative to their average positions $\mathbf{r}_n$ and the scattering amplitude of the modulated crystal is

$$S_{\text{mod}}(\mathbf{Q}) = F(\mathbf{Q}) \sum_n \exp[-i\mathbf{Q}\mathbf{r}_n + i\mathbf{Q}\mathbf{g}(\mathbf{r}_n)]. \quad (5)$$

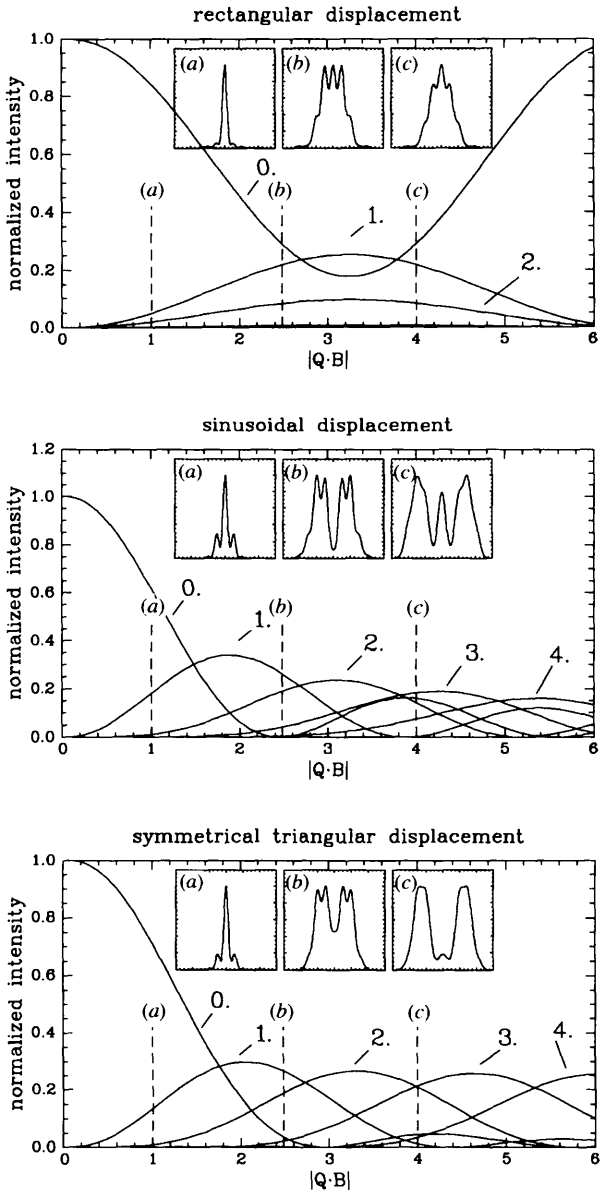

Fig. 2. The intensities of supersatellites of order n and of the main reflection ($n = 0$) calculated for three types of transverse displacement modulation: (I) rectangular displacement (symmetric case); (II) harmonic displacement; and (III) triangular displacement (symmetric case). The inserts give calculated Q scans for $|\mathbf{QB}| =$ (*a*) 1.00, (*b*) 2.50 and (*c*) 4.00 (compare with Fig. 5).

The function $\mathbf{g}(\mathbf{r}_n)$ describes the displacement (shape function) and is represented by a Fourier expansion:

$$\mathbf{g}(\mathbf{r}_n) = \mathbf{B}_0 \sum_{j=1}^{j_{\max}} c_j \sin(j\mathbf{Q}_{\text{mod}}\mathbf{r}_n) + d_j \cos(j\mathbf{Q}_{\text{mod}}\mathbf{r}_n).$$

$\mathbf{B}_0$ denotes the unit vector in the direction of the displacement amplitude $\mathbf{B}$, c_j and d_j are the respective Fourier coefficients. $j_{\max}$ is the maximum order of Fourier coefficients to be considered in the summation. Insertion into equation (5) yields

$$\begin{aligned} S_{\text{mod}}(\mathbf{Q}) &= F(\mathbf{Q}) \sum_n \exp\Big\{-i\mathbf{Q}\Big[\mathbf{r}_n - \mathbf{B}_0 \sum_{j=1}^{j_{\max}} c_j \sin(j\mathbf{Q}_{\text{mod}}\mathbf{r}_n) \\ &\quad + d_j \cos(j\mathbf{Q}_{\text{mod}}\mathbf{r}_n)\Big]\Big\} \quad (6) \\ &= F(\mathbf{Q}) \sum_n \exp(-i\mathbf{Q}\mathbf{r}_n) \\ &\quad \times \prod_{j=1}^{j_{\max}} \exp[i\mathbf{Q}\mathbf{B}_0 c_j \sin(j\mathbf{Q}_{\text{mod}}\mathbf{r}_n)] \\ &\quad \times \exp[i\mathbf{Q}\mathbf{B}_0 d_j \cos(j\mathbf{Q}_{\text{mod}}\mathbf{r}_n)]. \quad (7) \end{aligned}$$

Bessel functions of integer order can be introduced *via* (Abramowitz & Stegun, 1972)

$$\exp[ir\sin(\theta)] = \sum_{n=-\infty}^{\infty} J_n(r)\exp(in\theta) \quad (8)$$

$$\begin{aligned} \exp[ir\cos(\theta)] &= \sum_{m=-\infty}^{\infty} J_m(r)\exp[im(\theta + \pi/2)] \quad (9) \\ &= \sum_{m=-\infty}^{\infty} i^m J_m(r)\exp(im\theta) \end{aligned}$$

and we obtain

$$\begin{aligned} S_{\text{mod}}(\mathbf{Q}) &= F(\mathbf{Q}) \sum_n \sum_{n_1=-\infty}^{\infty} \sum_{n_2=-\infty}^{\infty} \cdots \sum_{m_{j_{\max}}=-\infty}^{\infty} J_{n_1}(c_1\mathbf{B}_0\mathbf{Q}) \times \cdots \\ &\quad \times J_{m_{j_{\max}}}(d_{j_{\max}}\mathbf{B}_0\mathbf{Q}) \exp\Big[(i\pi/2)\sum_{j=1}^{j_{\max}} m_j\Big] \\ &\quad \times \exp\Big[-i\mathbf{r}_n\mathbf{Q} + i\mathbf{r}_n\mathbf{Q}_{\text{mod}} \sum_{j=1}^{j_{\max}} (n_j j + m_j j)\Big]. \quad (10) \end{aligned}$$

The expression $\sum_n \exp[i(\mathbf{Q} + \mathbf{Q}_{\text{mod}} \sum_{j=1}^{j_{\max}} \ldots)\mathbf{r}_n]$ is a lattice function in three dimensions. It yields nonzero values $S_{\text{mod}}(\mathbf{Q})$ only for $\mathbf{Q} = \mathbf{G} + n\mathbf{Q}_{\text{mod}}$, where $\mathbf{G} = 2\pi(ha^*, kb^*, lc^*)$ (h, k, l integer values) is a lattice vector (in the present notation). Summation of all terms contributing to the same reflection finally leads to the

expression

$$S_{\mathrm{mod},n}(\mathbf{Q}) = F(\mathbf{Q}) \sum_{1,\ldots,j_{\max}}^{\infty} J_{n_1}(c_1\mathbf{B}_0\mathbf{Q}) \ldots \times J_{m_{j_{\max}}}(d_{j_{\max}}\mathbf{B}_0\mathbf{Q}) \exp\left[(i\pi/2)\sum_{j=1}^{j_{\max}} m_j\right] \quad (11)$$

with the restriction

$$\sum_{j=1}^{j_{\max}}(n_j + m_j)j = n, \quad n_j, m_j \text{ integers.}$$

The harmonic displacement function obviously is included in this description: Only the leading term $\sin(\mathbf{Q}_{\mathrm{mod}}\mathbf{r}_n)$ of the Fourier series is retained, and the restriction in equation (11) yields just one solution, namely $n_j = n$. Hence, the summation reduces to only one term and the same result as in equation (1) is obtained. In the general case, the restriction (11) in principle requires consideration of an infinite number of products of Bessel functions. Fortunately, most of them are negligibly small, since the Bessel functions of higher order have small values ($|J_n| << 1$) in the relevant $|\mathbf{Q} \cdot \mathbf{B}|$ range. Note that the satellites of order $\pm n$ are not necessarily of equal intensity.

3. Experimental details

Two samples were prepared from the same large crystal used by Burandt *et al.* (1992). From microprobe analysis, an average chemical composition of $An_{54}Or_4Ab_{42}$ was derived. (An = anorthite, Or = orthoclase, Ab = albite.) However, the observed blue schiller effect indicates a lower An content of 50 mol%. We obtained the following lattice constants: a = 8.185 (3), b = 12.874 (3), c = 14.232 (4) Å, α = 93.52 (2), β = 116.23 (2) and γ = 89.83 (2)°, refined from 28 centred reflections (λ = 0.56 Å).

The modulation vector was determined as $\mathbf{Q}_{\mathrm{mod}}$ = (−0.012, 0.060, 0.012) (average value), which corresponds to a period length of 1440 (70) Å. The scanning direction is that of the modulation vector, which has approximate direction $[\bar{1}51]$, in good agreement with the result of Burandt *et al.* (1992) and also with the values obtained by Bøggild's optical experiments (Bøggild, 1924). The step width (Δh, Δk, Δl) = (−0.001, 0.005, 0.001) was chosen to be small enough to make the best use of the mechanical accuracy of the instrument at the given wavelength (0.56 Å). This wavelength is large enough to resolve the intrinsic width of Bragg peaks and satellites and it also allows coverage of a large Q range. The satellite intensities for larger Q values are particularly important when investigating details of the modulation shape.

The experiments were performed with synchrotron radiation, at HASYLAB, Hamburg, on beamline D3 (four-circle diffractometer). The beamline is equipped with an Si(111) double monochromator, an Eulerian cradle and the operation is controlled by highly developed crystallographic software (Eichhorn, 1991) running on a MicroVax workstation. Measurements were performed in the Q-scan mode, which means for each measured reflection a scan on a straight line in reciprocal space through the main reflection and its supersatellites is performed. This method provides all the information about the respective intensities in one scan. Much care was taken in the resolution and optimum values were obtained by a reduced detector opening. Another effort was to find the best scattering geometry, considering the sample orientation and the anisotropic divergence of the synchrotron radiation at HASYLAB. The procedure is described in Appendix *A*.

First, Q scans were performed for all reflections within the range $\sin(\Theta)/\lambda < 0.46\,\text{Å}^{-1}$ (on sample I). The data were collected without optimizing the resolution along the radial direction (detector opening 4 × 4 mm and the usual data-collection conditions) in order to prevent alignment problems or errors in the orientation matrix. All reflections exhibited satellites and, generally, their intensity distribution was in good agreement with the earlier results of Burandt *et al.* (1992). The measurements were then extended to higher Q values. As shown in Appendix *A*, the parameter ψ was found to be of extreme importance for separating overlapping reflections. Since the modulation direction is $\simeq [\bar{1}51]$ and the amplitude vector roughly has the direction [10, 3, 8] (reciprocal-space coordinates), the Q dependence of satellite intensity should be visible best in the plane $h0l$ or $h\pm 1l$. For sample II, optimum ψ values are provided for these reflections. Thus, a small but well resolved data set of 140 reflections was collected for sample II. Here, the detector opening was reduced to 0.1 mm, enhancing resolution in the radial direction. About 800 reflections were measured. To demonstrate the data quality, three Q scans measured with optimum resolution (sample II) are shown in Fig. 3. They were selected in close correspondence with the three different regions discussed in Fig. 2 to illustrate the characteristics of the present measurements. The index of the reflections as well as the argument $|\mathbf{QB}|$, calculated for a sinusoidal displacement, is given in Fig. 2. Accordingly, the reflection $\bar{1}14$ corresponds to the insert denoted (*a*) in Fig. 2, $\bar{2}$,0,10 to (*b*) and $\bar{8}06$ to (*c*). Comparing the data, a rectangular displacement can be clearly ruled out, while both sinusoidal and triangular modulation functions show reasonable agreement.

4. Data analysis

Extracting the correct intensities is the main difficulty since the satellites are not always fully separable (see

Fig. 3). With increasing momentum transfer, the data are more and more difficult to interpret as the intensities are generally decreasing and the peaks broaden, too. For these reasons, numerous reflections were rejected in the analysis in a first run. 198 well resolved reflections remained and were fitted to the following model: A *Voigt profile* was taken for the main reflection (thus representing the experimental resolution) and a convolution of this Voigt profile with a Lorentzian for the satellites. The following restrictions were made in the fit:

(i) The distance between satellites of different order was kept fixed within each Q scan.

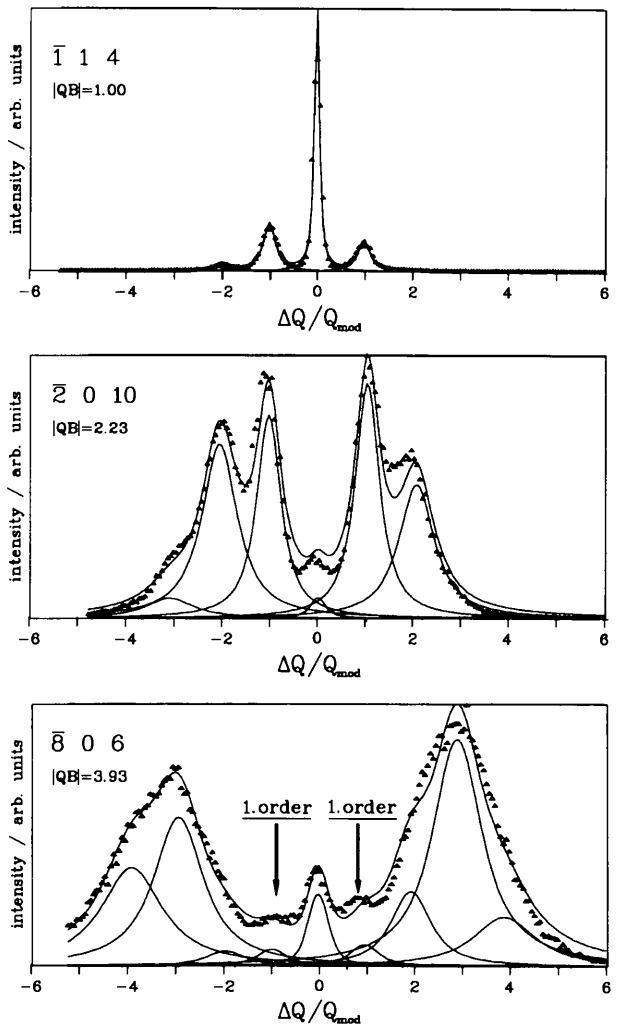

Fig. 3. The Q scans for the reflections $\bar{1}14$, $\bar{2},0,10$ and $\bar{8}06$ and the respective fits. Direct comparison with Fig. 2 suggests either a harmonic displacement or a triangular displacement. Note the difficulty of obtaining a unique fit for the reflection $\bar{8}06$, which is caused by decreasing resolution at larger momentum transfer. Also, note the asymmetries in intensities of satellites of order $\pm n$, the evidence of fourth-order satellites from the fitting curve for reflection $\bar{8}06$ and the positions of the first-order satellites, marked with arrows.

(ii) In a first step (sample I), the same intrinsic width was assumed for all satellites, since a fit of individual peak widths would increase the number of parameters. In the case of higher-order satellites (mainly sample II), a linearly increasing (Lorentzian) width was found to fit the measurements far better (see Fig. 3). This finding is discussed below.

Examples of the fits are shown in Fig. 3 (indicated by lines). A notable feature is a slight asymmetry of satellite intensities of order $\pm n$. As already mentioned, the asymmetry could be related to different widths of the two adjacent lamellae. Consequently, satellites of order $\pm n$ were treated separately in the fits. No errors of the intensity values are considered in the following. Implicitly, the data are treated as if the error was the same for all intensities. Within the theory in use, only relative intensities are exploited, which have values in the range between zero and unity (normalization to integrated intensities). Thus, the assumption of equal errors will not affect the results.

Since the rectangular wave clearly does not apply, the data were analysed within the scope of the Fourier expansion described in §2, equation (11), and within a triangular shape, equation (5). The ratio of satellite intensities and the main reflection intensities $I_{\mathrm{sat},n}/I_{\mathrm{MR}}$ has been used as a fundamental quantity by Burandt *et al.* (1992). In the case of main reflections of zero intensity, the normalization to I_{MR} causes artificial poles [see Fig. 5 of Burandt *et al.* (1992)], creating some inconvenience. In the present paper, we therefore suggest a normalization to the *integrated* intensity $I = \sum_{n=-\infty}^{\infty} I_{\mathrm{sat},n}$ ($n = 0$ denoting the main reflection). For a pure displacement modulation, this is a reasonable choice, since the completeness of the Fourier expansion yields $I = |F_0|^2$ for any Fourier series. In both normalizations, the knowledge of the exact (unmodulated) structure factor and its Q dependence is not required for the data analysis. Additionally, in both cases, no Lorentz/polarization corrections are necessary.

Within the approach of equation (11), the transverseness of the modulation was assumed *a priori*. To reduce the number of parameters in the fit, only the modulus of amplitude B and its direction are adapted. The latter is given by the angle between **B** and **c***. Successively, higher-order harmonics were included in the expansion for B. The results are given in Table 1. The most important reduction in χ^2 [$= \sum(I_{\mathrm{obs}} - I_{\mathrm{calc}})^2$] occurred after introducing the third term of the Fourier expansion. The expansion coefficient $c_3 = -0.0605$ has the same sign as the corresponding term of the Fourier series for the triangular modulation: $g(x) = 1\sin(x) - 1/9\sin(3x) + 1/25\sin(5x) - 1/49\sin(7x) + \ldots$. The observed coefficient c_4 introduces significant asymmetry, while the higher Fourier components do not affect the fit quality and thus are not significant. Cosine terms (d_i) were checked also, but were found to be insignificant. The fit results are illustrated in Fig. 4. They are compared with

Table 1. *Fourier coefficients of fits to the intensity data, successively including higher-order Fourier components (up to seventh order)*

In Fig. 6, the normalized intensities are indicated with crosses. The expansion contains sine terms only. The modulation function is given as $g(\mathbf{r}) = B_0 \sum_l c_l \sin(l\mathbf{Q}_{\rm mod}\mathbf{r})$ with $c_1 = 1$. As can be seen from the evolution of the value of χ^2, the introduction of c_3 was most effective. The parameters obtained from a fit with the triangular modulation are also listed.

Fourier expansion

Coefficient	B (Å)	c_2	c_3	c_4	c_5	c_6	c_7	χ^2
1	0.46	–	–	–	–	–	–	3.437
2	0.46	−0.011	–	–	–	–	–	3.405
3	0.48	−0.011	−0.061	–	–	–	–	2.497
3*a*	0.48	–	−0.058	–	–	–	–	2.527
4	0.48	–	−0.061	0.016	–	–	–	2.483
4*a*	0.48	−0.0067	−0.060	0.0128	–	–	–	2.475
5	0.48	–	−0.061	0.017	−0.004	–	–	2.476
5*a*	0.48	−0.0065	−0.060	0.0126	−0.007	–	–	2.468
7	0.48	–	−0.060	0.0165	–	–	0.0064	2.483

Triangular model

B (Å)	D_1/M	χ^2
0.60	0.49	2.970

the measured data for intensities of the main reflections as well as first-, second- and third-order satellites. The fit for the harmonic displacements is indicated by lines, while the result including higher harmonics up to fifth order is indicated by full circles. Additionally, the result for a purely triangular displacement is given (dashed lines). Following the fit results in Table 1, the latter curves were calculated for a small asymmetry ($D_1/M = 0.49$). In the regime of small arguments $|\mathbf{QB}_0|$, the harmonic approach is sufficient. For larger arguments, both the Fourier expansion and the triangular model give somewhat better agreement. The actual displacement functions are hardly distinguishable, though. In Fig. 5, they are illustrated with the same symbols and lines as in Fig. 4. The displacement amplitude is 0.60 Å, based on the triangular displacement modulation or 0.48 Å, utilizing the Fourier expansion with direction $\approx [10, 3, 8]$ (reciprocal-space coordinates, smallest integer values). The result is identical to $\mathbf{B} = 0.063a + 0.001b + 0.017c$. The amplitude is smaller than the value of Burandt *et al.* (1992) but still quite large. Its direction, which is determined more accurately here, deviates 16° from the value given by Burandt *et al.* (1992).

The results obtained with the *JANA*94 program for a similar simple model (only first- and third-order harmonics for the complete unit contents, no cosine terms) are in good agreement: The amplitude vector ended up with amplitude values $x \sin 1 = 0.0639\,(3)$, $y \sin 1 = 0.0012\,(6)$, $z \sin 1 = 0.0261\,(3)$ and $x \sin 3 = -0.0038\,(4)$, $y \sin 3 = 0.0003\,(8)$, $z \sin 3 = -0.0011\,(4)$.

A list of observed and calculated parameters has been deposited.* An overall R value of roughly 17% was obtained, which can be reduced further (down to 13%) by allowing further degrees of freedom. The corresponding results were, however, not fully reliable but allow some hints to further discussion (see below).

5. Discussion

The relatively good fit, as shown in Table 1 and Fig. 4, confirms that our simple model of a purely transverse displacive modulation of the entire unit cell does indeed reflect the main characteristics of the s-type superstructure. A new and essential result concerns details of the displacement function. Agreement with a purely sinusoidal displacement modulation is quite good, while a rectangular shape can definitely be ruled out. Introduction of higher-order Fourier components shows that the displacement is anharmonic with the third-order coefficient relatively large and similar to that of a triangular modulation.

Although the test refinements with *JANA* did not provide any really significant results concerning individual modulations of the atoms, some of them showed a 'general tendency', which may at least serve as a basis for further discussion. As expected and in agreement with TEM (Hoshi, Tagai & Suzuki, 1996) and ion-probe measurements (Miúra & Tomisaka, 1978), there is a modulation of the occupancy of the Na/Ca sites. These M sites are usually found to be split roughly along $[0\bar{5}3]$ in the *average* structure of intermediate plagioclases (Fitzgerald, Parise & Mackinson, 1986). As mentioned, this averaging relates to the e-modulation, but *not* to the s-modulation, for which an ideal unmodulated structure is refined. Our test refinements showed a tendency towards an antiphase occupational modulation of the two sites. In addition, allowing individual displacements for the two M sites showed that the x and z components are

* Lists of raw data, observed and calculated intensities, refined parameters and fit restrictions have been deposited with the IUCr (Reference: JS0050). Copies may be obtained through The Managing Editor, International Union of Crystallography, 5 Abbey Square, Chester CH1 2HU, England.

roughly equal to those of the (rigid) Si/Al–O framework, while the y component (which is negligibly small for the framework) is large and again in antiphase between the two sites. So, an alternating occupancy of the two sites in the two s-lamellae might provide an explanation for the well known finding of split M sites in plagioclases.

The observed nearly triangular shape function for the s-modulation can be explained as follows (see Fig. 1*b*): The different An content in the two lamellae leads to slightly different lattice constants. In order to reduce the strains at the interfaces, the lamellae are slightly tilted relative to each other. This idea has already been put forward by Olsen (1977, 1979) who derived different lattice parameters for the two Bøggild lamellae from TEM measurements, and with the TEM image in Wenk & Nakajiama (1988; see also Smith & Brown, 1980). Olsen (1977) reports a difference in the lattice angle γ of $\Delta\gamma = 0.17°$. This value leads to a displacement amplitude of $1500\,\text{Å} \times \frac{1}{4} \sin 0.17° = 1.11\,\text{Å}$, a value larger than ours but of the same order of magnitude. Some of the departure from a triangular displacement function can be attributed to the method: X-ray scattering averages over a large area in real space and samples a limited number of Fourier components. Contributions of lamellae with varying width smooth the resulting displacement function.

Finally, the line width of the satellite reflections is discussed. It is considerably larger than the width of the main peaks. The latter has been used as the experimental resolution. Here, effects like the mosaicity of the sample are already included. The additional width of the satellites is obtained by a deconvolution and results from the limited range and imperfections of the superstructure. For the best resolved scans of sample II, the intrinsic satellite widths were extracted. As already evident from Fig. 3, the satellite width increases linearly with the satellite order n. The average experimental values are presented in Fig. 6: It yields a straight line with a slope of $1.3\,(2) \times 10^{-3}\,\text{Å}^{-1}$. With the inverse width taken as the range of the correlation, a value of about 5000 Å is obtained from the first-order satellites. This value is small compared with the period of the lamellar superstructure.

A linear increase is characteristic of strains. There is no size effect, which should yield an additional constant contribution, and no short-range or paracrystalline behaviour, which should lead to a quadratic increase. The corresponding strain

$$\frac{\Delta l_s}{l_s} = \frac{\Delta Q_{mod}}{Q_{mod}} = \frac{1.3 \times 10^{-3}}{4.35 \times 10^{-3}} = 0.30$$

is very large (l_s = thickness of lamellae) and appears

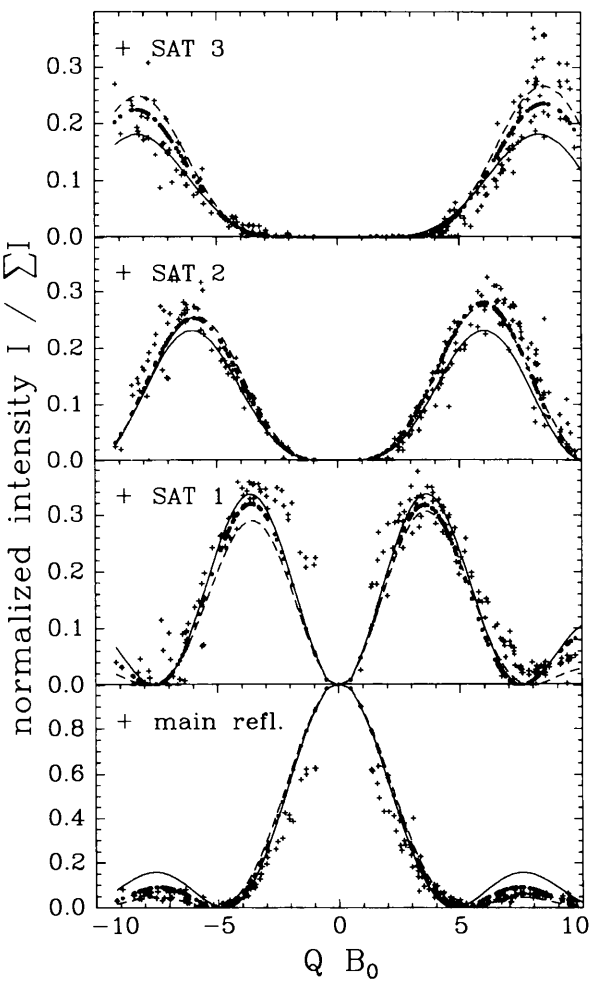

Fig. 4. Relative intensities of the measured satellites (+ + +), $I_{sat,n}/I$ with $I = \sum_{n=-\infty}^{\infty} I_{sat,n}$, denoting the integrated intensities, fitted by the triangular model (– – –), the harmonic model (——) and the Fourier expansion (· · · · ·). The main reflections, first-, second- and third-order satellites are displayed separately ($\mathbf{B}_0 = \mathbf{B}/|B|$).

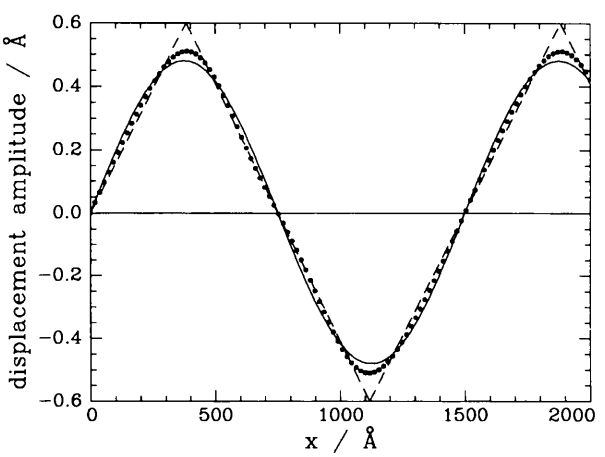

Fig. 5. The displacement functions describing the modulation. They correspond to the fits in Fig. 4 for the analytical triangular displacement (– – –), the harmonic displacement (——) and the Fourier expansion (· · · · ·). The parameters are given in Table 1.

implausible as a homogeneous strain field of very long range.

We therefore developed a model for the profiles taking into account varying lamellar thicknesses with small finite sizes. Within such a model, an average roughness of 480 Å is derived, which is a realistic average value when integrating over the whole sample. Assuming perfect ordered packages, this large average roughness invalidates the approximation of the profiles by simple Lorentzians. In fact, the superposition of individual Laue functions gives much better fits. A more detailed profile analysis of the data within this model is in progress.

APPENDIX A
Optimizing resolution in the Q-scan mode

The Q-scan mode allows scans along linear rods in reciprocal space. Owing to the anisotropic resolution at HASYLAB beamline D3, a Q scan with arbitrary sample orientation does not always provide the best resolution. This is shown in Fig. 7(*a*) for the Q scan on reflection $\bar{6}06$. The ψ *rotation* offers a strategy for optimizing the resolution in Q scans, as illustrated below. For the possibility of an arbitrary sample rotation using the Eulerian cradle, there is in principle an infinite number of settings for the diffractometer angles χ, φ and ω, which satisfy the scattering condition. For a given reflection *hkl*, this is illustrated by use of the parameter ψ, denoting a rotation about the scattering vector. By default, the Q scan is normally done at $\psi = 0°$, which represents the bisecting mode ($\omega = 2\theta/2$). The choice of ψ is a crucial point concerning the measurements, its influence on the experimental results is illustrated in Fig. 7 using the example of $\bar{6}06$ reflection. In the genuine Q scan of the reflection $\bar{6}06$ with $\psi = 0$, the supersatellites are not well resolved (Fig. 7*a*). A series of ω scans with different ψ values is shown in Fig. 7(*b*). For $\psi = 230°$, the satellites are clearly separate but, for $\psi = 160°$, the satellites remain completely unresolved. Instead, an increased intensity is obtained, originating from the integration over the main reflection and the supersatellites. The anisotropic resolution window in the '$|\mathbf{Q}|$ = constant' plane and the meaning of ψ are illustrated in Fig. 7(*c*). From this sketch, the importance of an optimum ψ value becomes obvious, both for a Q scan along the satellite vector and for the ω scan. An optimum choice for ψ definitely improves the quality of the data.

{It would have been better to perform Q scans with different ψ values in Fig. 7(*b*) but this option was not available at the time of this measurement. From the anisotropic resolution function at the instrument, the ω scan in the present case contains the same information as the Q scan, as the satellite vector (direction $[\bar{1}51]$) is almost perpendicular to $\bar{6}06$.}

The best ψ value can be derived using the basic diffractometer equation as given *e.g.* in Eichhorn (1991) or in Busing & Levy (1967):

$$\mathbf{V}_{\rm diff} = \Psi(\psi)R_0(hkl)UB(hkl). \qquad (12)$$

$\mathbf{V}_{\rm diff}$ is the diffraction vector, Ψ is the ψ-rotation matrix, R_0 is the instrumental angle matrix (bisecting case) and UB the sample orientation matrix. The equation is

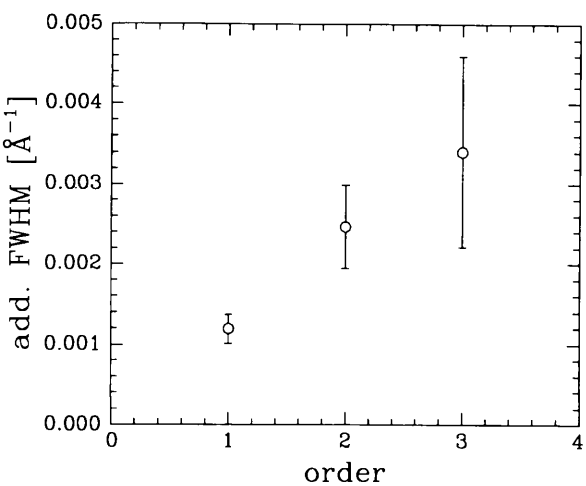

Fig. 6. The intrinsic width of the satellites of order n obtained after deconvolution. The data suggest a linear broadening with increasing satellite order. A slope of 1.3 (2) Å^{-1} is found.

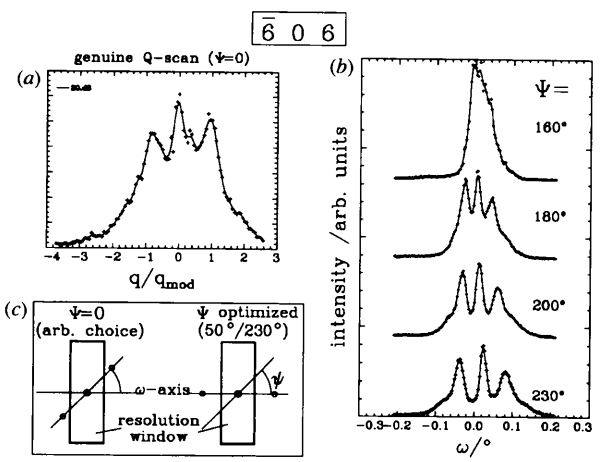

Fig. 7. (*a*) Genuine Q scan for reflection $\bar{6}06$, recorded in the bisecting mode ($\psi = 0$, as explained in the text). (*b*) ω scans for different values of ψ for the same reflection. The satellites are best resolved in the ω scan with $\psi = 230°$. (*c*) Illustration of the scattering geometry for different ψ values. The sketch shows the Q-space plane perpendicular to the scattering vector of the main reflection. The box illustrates the anisotropy of the resolution window and the large circle inside the resolution window denotes the main reflection, which is symmetrically surrounded by two satellite reflections. When $\psi = 0$, the orientation of the scanning direction is arbitrary with respect to the resolution window, while, for an optimum ψ value, the satellites can be separated more easily, both in the ω scan and in the Q scan.

normally used to calculate the settings of the instrumental angles for the reflection *hkl*. Somehow, calculating $\mathbf{V}_{\rm diff}$ for the scanning direction $\mathbf{q}_{\rm mod} = [\Delta h \Delta k \Delta l]$ contains information about the scanning geometry. With the optimum choice for ψ, the third component of the diffraction vector $\mathbf{V}_{\rm diff}(3)$ is zero in the equation

$$\mathbf{V}_{\rm diff} = \Psi(\psi) R_0(hkl) UB[\Delta h \Delta k \Delta l]. \qquad (13)$$

This means that the sample is rotated around the scattering vector *hkl* until the vector $(\Delta h \Delta k \Delta l) = \mathbf{Q}_{\rm mod}$ reaches the basal plane of the Eulerian cradle. With proper account for the anisotropic divergence of the synchrotron-radiation beam at HASYLAB, optimum resolution is obtained in the basal plane. The effect of an optimum choice for ψ in the Q-scan mode is demonstrated in Fig. 8. Q scans ($\psi = 0$) of reflection 600 for two samples with different orientation are shown. The optimum ψ value was calculated as 133° for sample I, while it is 8° for sample II. As expected, for sample II and the Q scan with $\psi = 0°$, the satellites are far better resolved than for sample I. The Q scan can be performed with a selected ψ value too but, owing to the large shading regions of the Eulerian cradle, the optimum scan is not always possible without an appropriate preorientation of the sample.

We are indebted to Dr K.-F. Hesse (Institut für Kristallographie, Universität Kiel), for help in preparation of sample I, to Dr G. Adiwidjaja (Institut für Mineralogie, Universität Hamburg) for the preparation of sample II and to A. Richter (Universität Kiel) for providing the mother crystal. Many thanks are owed to Dr P. M. Sachs (GEOMAR, Kiel) for the microprobe analysis and Sebastian Körber, Herwig Requardt and Wolfgang A. Caliebe for assistance during the measurements. Dr K. Eichhorn and Dr H. G. Krane provided a perfectly running X-ray diffraction machine at HASYLAB D3. The data analysis was performed with the program packages *LSFIT* (Nöldeke, Seeck, Grieger & Nitz, 1995) and *JANA* (Petříček, 1994). It is a pleasure to thank Oliver H. Seeck (Institut für Experimentalphysik, Universität Kiel) and Dr Vaclav Petříček for their kind support. The Deutsche Forschungsgemeinschaft is acknowledged for financial support within the Schwerpunktprogramm 'Pseudosymmetrie'.

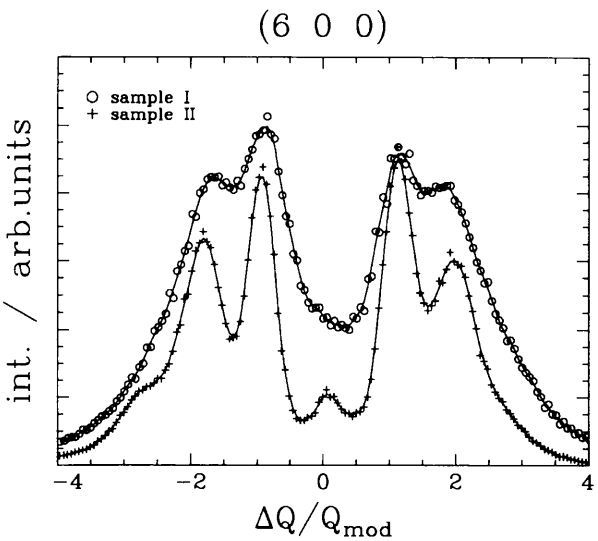

Fig. 8. The Q scan on the reflection 600, recorded for two different samples. The quality of the Q scan is far better for sample II, since the preorientation of the sample leads to an optimum ψ value of 8°, while for the 600 reflection of sample I the optimum choice would have been 133°. Since the Q scan was recorded in the bisecting mode, a value close to 0 or 180° provides optimum resolution for this scan.

References

Abramowitz, M. & Stegun, I. A. (1972). *Handbook of Mathematical Functions*. New York: Dover Publications.
Bøggild, O. B. (1924). *K. Dan. Vidensk. Selsk. Mat. Fys. Medd.* **6**, 1–79.
Böhm, H. (1976). *Z. Kristallogr.* **143**, 55–66.
Böhm, H. (1977). Habilitationsschrift, Universität Münster, Germany.
Burandt, B., Komorek, M., Press, W. & Boysen, H. (1992). *Z. Kristallogr.* **200**, 141–156.
Busing, W. R. & Levy, H. A. (1967). *Acta Cryst.* **22**, 457–463.
Eichhorn, K. (1991). *DIF4 User's Guide*. HASYLAB, DESY, Hamburg, Germany.
Fitzgerald, J. D., Parise, J. B. & Mackinson, I. D. R. (1986). *Am. Mineral.* **71**, 1399–1405.
Horst, W., Tagai, T., Korekawa, M. & Jagodzinski, H. (1981). *Z. Kristallogr.* **157**, 233–250.
Hoshi, T., Tagai, T. & Suzuki, M. (1996). *Z. Kristallogr.* **211**, 879–883.
Jagodzinski, H. (1984). *Bull. Minéral.* **107**, 455–466.
Jagodzinski, H. & Korekawa, M. (1965). *Naturwissenschaften*, **23**, 640.
Janner, A. & Janssen, T. (1977). *Phys. Rev. B*, **15**, 643.
Kek, S., Boysen, H., Kalning, M., Dorna, V., Press, W. & Adiwidjaja, G. (1995). *Die modulierte Struktur des Labradorits*, HASYLAB Annual Report, p. 429. HASYLAB, DESY, Hamburg, Germany.
Kek, S., Kalning, M., Press, W., Boysen, H. & Frey, F. (1997). *Z. Kristallogr.* **12**, 172.
Korekawa, M. (1967*a*). *Schweiz. Mineral. Petrogr. Mitt.* **47**, 269–278.
Korekawa, M. (1967*b*). Habilitationsschrift, Universität München, Germany.
Lam, J. W., Beurskens, P. T. & van Smaalen, S. (1994). *Acta Cryst.* A**50**, 690–703.
Miúra, Y. & Tomisaka, T. (1978). *Am. Mineral.* **63**, 584–590.
Nöldeke, C., Seeck, O. H., Grieger, S. & Nitz, V. (1995). *LSFIT, a Flexible Least-Squares Fitting Program Package*. Institut für Experimentalphysik, Universität Kiel, Germany.
Olsen, A. (1977). *Acta Cryst.* A**33**, 706–712.
Olsen, A. (1979). *Phys. Chem. Miner.* **4**, 115–127.
Petříček, V. (1994). *JANA*94, *Programs for Modulated and Composite Crystals*. Institute of Physics, Praha, Czech Republic.

Petříček, V., Maly, K., Coppens, P., Bu, X., Cisarova, I. & Frost-Jensen, A. (1991). *Acta Cryst.* A**47**, 210–216.
Smith, J. V. & Brown, W. L. (1980). *Feldspar Minerals*, Vol. 1, Fig. 19.31. Berlin: Springer Verlag.
Toman, K. & Frueh, A. J. (1976). *Acta Cryst.* B**32**, 526–538.
Wenk, H. R. & Nakajima, Y. (1988). *Phys. Chem. Miner.* **6**, 169–186.
Wolff, P. M. de (1974). *Acta Cryst.* A**30**, 777–785.
Wolff, P. M. de (1977). *Acta Cryst.* A**33**, 493–497.
Wolff, P. M. de, Janssen, T. & Janner, A. (1981). *Acta Cryst.* A**37**, 625–636.
Yamamoto, A. (1982*a*). *Acta Cryst.* A**38**, 87–92.
Yamamoto, A. (1982*b*). *Acta Cryst.* B**38**, 1446–1451.
Yamamoto, A., Nakazawa, H., Kitamura, H. & Morimoto, N. (1984). *Acta Cryst.* B**40**, 228–237.